Effect of α-stable sorptive waiting times on microbial transport in microflow cells

F. Alejandro Bonilla* and John H. Cushman†

Departments of Mathematics and Agronomy, Center for Applied Mathematics, Math Sciences Building, Purdue University, West Lafayette, Indiana 47907

(Received 13 December 2001; revised manuscript received 22 April 2002; published 27 September 2002)

The interaction of bacteria in the fluid phase with pore walls of a porous material involves a wide range of effective reaction times which obey a diversity of substrate-bacteria adhesion conditions, and adhesive mechanisms. For a transported species, this heterogeneity in sorption conditions occurs both in time and space. Modern experimental methods allow one to measure adhesive reaction times of individual bacteria. This detailed information may be incorporated into nonequilibrium transport-sorption models that capture the heterogeneity in reaction times caused by varying chemical conditions. We have carried out particle (Brownian dynamic) simulations of adhesive, self-motile bacteria convected between two infinite plates as a model for a microflow cell. The adhesive heterogeneity is included by introducing adhesive reaction time (understood as time spent at a solid boundary once the particle collides against it) as a random variable that can be infinite (irreversible sorption) or vary over a wide range of values. This is made possible by treating this reaction time random variable as having an α-stable probability distribution whose properties (e.g., infinite moments and long tails) are distinctive from the standard exponential distribution commonly used to model reversible sorption. In addition, the α-stable distribution is renormalizable and hence upscalable to complex porous media. Simulations are performed in a pressure-driven microflow cell. Bacteria motility (driven by an effective Brownian force) acts as a dispersive component in the convective field. Upon collision with the pore wall, bacteria attachment or detachment occurs. The time bacteria spend at the wall varies over a wide range of time scales. This model has the advantage of being parsimonious, that is, involving very few parameters to model complex irreversible or reversible adhesion in heterogeneous environments. It is shown that, as in Taylor dispersion, the ratio of the channel half width b to the Brownian bacteria motility coefficient (D_0 or dispersion coefficient) $t_b = b^2/D_0$ controls the different adhesion regimes along with the value of α. Universal scalings (with respect to dimensionless time $t_* = t/t_b$) for the mean position, $\langle X \rangle = V^*_{\text{eff}} t^{\theta}_*$, and mean-square displacement, $\langle \Delta X^2 \rangle = D^*_{\text{eff}} t^{\gamma}_*$ exist for long-time dispersion and the coefficients were obtained. The model can account for a great many sorptive processes including reversible and irreversible sorption, and sub- and superdispersive regimes with just a few parameters.

DOI: 10.1103/PhysRevE.66.031915 PACS number(s): 87.10.+e

I. INTRODUCTION

The present study is motivated by the desire to predict the spread of genetic information through complex natural porous media. Specifically, our group is interested in verifying the two following hypotheses: (i) Newly introduced bacteria can exchange specific genes with indigenous species that are attached to a surface provided the genes are judiciously located in the genome of the donor bacterium. Under this hypothesis, the survival of the newly introduced bacterium is unimportant provided the genes of interest are transferred to the indigenous species. (ii) Given information on the ''stickiness'' and hydrodynamic characteristics of the indigenous and introduced populations, it is possible to mechanistically predict the success of gene transfer strategies in porous media. This later hypothesis is partially addressed by the work presented herein, that is, this is a first step in verification of hypothesis (ii). A first step in verification of hypothesis (i) may be found in Wu [1].

Bacterial motility is of importance to a wide spectrum of applied scientific disciplines, including human health, food science, and environmental bioremediation. Analysis of microbe dynamics is far from complete. The phenomena found is as diverse as life itself [2,3], involving mechanisms of bacteria motility, bacteria-substrate (surface) and cell-to-cell interactions, hydrodynamic interactions, chemotaxis, thermotaxis, magnetotaxis, and adhesion. These mechanisms act on spatial scales ranging from nanometers to millimeters. To understand the mechanisms of bacterial motility, one needs knowledge from several scientific disciplines: anatomy, genetics, chemistry, and physics [2].

An important factor in the engineering of biobarriers or bioremediation is the microbial partitioning that takes place between the aqueous and solid phases. Factors that affect such partitioning are numerous, but include such things as growth and starvation conditions [4–6], limiting of nutrients [7], potential toxicity in the aqueous phase [8], as well as varying surface properties of the adsorbent. The proper representation of the biological phase is a matter without consensus (as noted in the exchanges of Widdowson [9] and Jaffe and Taylor [10]). We present a model which will serve as a basis for an unstructured biological population, and will focus on the individual dynamics of a single microbe, or a system of such particles in relatively low concentration so

*Now at Department of Chemical Engineering, Purdue University.

†Email address: jcushman@purdue.edu

that they have little effect on the surrounding environment and each other. One may think of this as the initial stage before a type of colonization of the surface occurs.

Before we focus on the main aspects of this study, we briefly refer to some of the most relevant research on the subject. Although several references and models are mentioned in the Introduction, no excessive details are given since there exist in the literature good reviews on the subject [2,11].

A. Relevant scales

In a single microflow cell, at least three different length scales need to be explored. Within tens of nanometers (submicron scale) from the pore wall, bacterium-wall interactions will dominate over diffusion or convection. On the scale of several bacterium radii (a few microns), hydrodynamic interactions between the microbe and the surface and other particles, bacterial motility, and reduced diffusion dominate. At the scale of the pore radius (tens of microns to millimeters), convection, bacterial motility, hydrodynamic dispersion, and diffusion in the bulk phase combine to affect transport.

Associated with each length scale, there, exists a time scale which plays an important role in this biophysical transport problem and consequently in designing an efficient Brownian dynamics computational algorithm. We discuss this and the various processes in subsequent sections.

B. Bacterial motility and advection

The movement of bacteria in a stagnant fluid is described by a run and tumble (or twiddle) behavior [2,12]. This behavior consists of a sequence of runs, that is, a linear movement in a particular direction, followed by tumbles which are random changes of direction. While the length of the jumps in the motility pattern seems to be better described by a Levy flight random search [2,13], it has been modeled as a Brownian motion in the present work. The diffusion coefficient is associated with bacteria self-propulsion rather than a thermal bath. Brownian dynamics seem to describe such a motility pattern in certain cases, and a number of studies [14,15] support its use for modeling bacteria motility. The classical Brownian diffusion coefficient is replaced with a larger coefficient representing bacteria self propulsion. This assumes the run and tumble mechanism has a similar probability law or limit theorem to that of a larger particle in a bath of many identical, smaller particles. The random forces can be thought of as a sum of Brownian forces together with random swimming forces generated by a microbe in a homogeneous liquid. If there is no chemo-, thermo-, or magnetotaxis then the angular diffusion is isotropic. We assume the random forces are normally distributed and independent. The normality assumption is an averaging over different particle trajectories. Swimming bacteria patterns may exhibit specific features different from those of Brownian dynamics. Kuo and McGrath [16], for instance, dispute the validity of Brownian models applied to bacterial transport based on observed fluctuations of Listeria motility.

Most research on bacterial motility has centered on flagellated organisms, like *E. coli*. Berg and collaborators have explained how flagellated cells swim and how their molecular sized engines work [2]. Only recently significant findings about nonflagellated organisms have emerged [17]. Nonflagellated microbes are thought to move by producing traveling waves that propagate down the surface of the microbe. Samuel *et al.* [17] have discovered fine hairs just a few nanometers thick and a fraction of a micrometers long surrounding a cyanobacterium. This finding enhances the wave propagation theory and provides a better explanation based on fine hair self propulsion.

Biondi *et al.* [18] studied swimming bacteria (*E. coli*) in restricted geometries, measuring cell velocity, tumbling probability, and turn angle of single cells in micro channels. They concluded that only when capillaries are smaller than three times the diameter of the bacteria, there exist a visible change in the bacteria's motility with respect to their motility in a bulk fluid (unrestricted media). The macroscopic motility in unrestricted geometry with respect to motility in very small capillaries is increased by a factor proportional to the size of the system. By design, sticking to the glass surfaces did not occur in their experiments.

Phillips *et al.* [19] measured in separate experiments the motility of *E. coli*. They determined the distribution of cell velocities was slightly skewed from normal, and the run length time distributions were exponential. They were unable to measure turn angles between consecutive runs because cells would not remain in the microscope's focal plane long enough. The values of the variables that could not be measured were taken for their analysis from Berg and Brown [20]. They also suggested that the macroscopic behavior of population motility can be predicted from microscopic observations. In particular, the expressions proposed by Othmer *et al.* [21], and Rivero *et al.* [22] were suitable for the conditions tested.

The behavior of motile cells near a solid surface has been extensively studied experimentally in the absence of bulk flow, but relatively little is known about motile cell behavior in advective flow fields [23]. Camesano and Logan [23] studied the effect of fluid velocity on the transport of motile and nonmotile bacteria. They observed that the collision efficiency (defined as the ratio of particles that attach to soil grains to particles that collide with the soil) decreases as the mean velocity decreases. An alternative definition of collision efficiency closer to what is presented here is that given by Rijnaarts *et al.* [24]: Collision efficiency is the probability of a cell to attach upon reaching a substratum. This may be computed as the ratio of collisions where particles attach to soil grains, to total number of collisions against the soil. Testing against nonmotile bacteria, they hypothesize that swimming cells are able to avoid sticking to soil grains at low-fluid velocities, while at high-fluid velocities, bacteria could not reduce attachment. The present work examines in virtual experiments the movement of single-cell organisms subject to convective flow and fluctuations driven by Brownian dynamics. The fluctuations owe their origin to the swimming character of the microbe. It also includes attachment and detachment from the walls including reversible and irreversible sorption.

C. Bacterial adhesion

Researchers looking at bacterial adhesion have used knowledge developed studying the sorption of macromolecules or colloidal particles to formulate theories and devise experimental methods. In the development of sorption theories, irreversible sorption has been more actively researched than reversible sorption. This is in part because for many applications (e.g., filtration) sorption is irreversible. Another reason is that the irreversible problem is easier to analyze. A perfect sink wall or irreversible sorption boundary [11] produces a system of equations for which solutions are known. A reversible sorbing boundary produces a far more complex system of coupled equations for which solutions are often not readily available [11,25]. Sorption to a reversible boundary depends on the history of sorption (another type of steric effect), which in turn depends on phenomena occurring in the bulk phase. The result is a nonlinear behavior.

Bacteria often reversibly attach to mineral and biological surfaces [3,26–29]. More experimental observations are necessary to define the characteristics of residence times and the effect of conditions such as stress (e.g., starvation conditions), chemical gradients (chemotactic behavior), hydrophobic or hydrophilic effects, etc. Adhesion strength is time dependent; adhesion may be reversible until a point in time in which the attachment becomes irreversible [28–30].

It has been proposed that once a cell has arrived within a few nanometers from a wall with an attractive potential, it will be sorbed irreversibly [30,31]. Yet, when sorbed there remains a possibility for lateral displacement [31] over distances of several particle diameters. This lateral translation coupled with the existence of heterogeneities over the substrate may affect desorption. Upon arrival to positions where the attractive potential decreases, bacteria might be able to free themselves from the adsorbent's surface and swim into the aqueous phase.

D. Brownian dynamics simulations

Brownian dynamics provides a rigorous dynamical model sophisticated enough to study the rich behavior of bacterial transport including sorption. Dealing with various boundary conditions is not a trivial exercise when studying Brownian particles. While ''sticky'' Brownian motion has been studied in the mathematical literature, it has not been applied to sorption. A large part of the Brownian dynamics simulation work analyzing hydrodynamic interactions between particles and walls is based on an algorithm by Ermak and McCammon [32] (see also Bafaluy *et al.* [33]).

The Brownian dynamics computation presented here incorporates the effect of reversible adhesion through the use of sticky Brownian motion. The focus is on the single pore scale. This task also involves processes at two additional length scales, that is, a diffusive layer extending a few microns from the substrate surface and an sorptive or interaction layer of submicron thickness. No model for these two smaller scales is presented. Instead, a stochastic process is hypothetically formulated that is consistent with the transport properties observed in experiments and what is known in theory and practice about the processes involved at those scales. With this, the algorithm centers on the effects of reversible and irreversible adhesion at the pore scale, and *the effects of bacteria motility*.

The transport of a Brownian particle sticking to a wall is analyzed under advection by a Couette flow between infinite planes. Laminar or creeping flow is the focus of the hydrodynamic study, since the natural system (water flow in geological formations) of interest exhibits low Reynolds numbers and as such is rarely if ever turbulent. The bacterial trajectories are modeled and statistical averages are computed and discussed. The bacteria are modeled as Lagrangian particles subject to drag and self-propelling (swimming) forces. These forces are generally unknown, yet phenomenological and statistical information merits modeling them as random. Brownian motion seems an appealing model for bacterial swimming, and it is coupled to a probabilistic wall attachment or detachment model. This probabilistic model introduces stickiness parameters to control the attachment or detachment process or physicochemical interactions between microbes and the solid matrix. Bacteria sorption is a composition of processes on many time scales. Dominant adhesive processes may be ruled by short time in the diffusive layer and longer-time adhesion associated with the submicron scale. When the substrate conditions are variable in space, and the bacteria itself exhibits heterogeneity in the attaching conditions or mechanisms, one might expect that for many collision or attachment events, the distribution of waiting times will look continuous instead of appearing multimodal or discrete.

II. MODEL

Here we discuss the mathematical model for the transport of bacteria in solution which react with a solid surface (adsorbent) containing the solution. Mathematically, the volume occupied by the solution is labeled free space or domain and the solid surface is the domain boundary. Bacteria possess search mechanisms [13] which are manifest in motility composed by run and tumbles as discussed in the introduction. Bacteria respond to stimuli (e.g., a chemical, thermal, or magnetic gradient in which case the phenomenon are known as chemo-, thermo- or magnetotaxis, respectively) by increasing or decreasing run times between tumbles. The actual tumbling distribution appears unaffected by the environment. If a chemical potential is introduced into a medium containing bacteria, receptors on the microbe surface can detect the change up to a saturation point at which all receptors are activated. In a large population of bacteria, a statistical average can be made for the concentration in the presence of a one-dimensional gradient. This homogenization performed in Rivero *et al.* [22] leads in one dimension to a classical convective-dispersion equation (CDE) and if there is no gradient in chemical potential then the CDE reduces to a classical diffusion equation with the diffusion coefficient representative of the random run and tumbling.

If we think of the concentration of microbes, $C(x,t)$, as a probability density, $p(t,x)$, we can write the CDE as

$$\frac{\partial p}{\partial t} = \frac{\partial}{\partial x}\left[D(x,t)\,\frac{\partial p}{\partial x}\right] - \frac{\partial}{\partial x}[V(x,t)p], \tag{1}$$

which corresponds to a forward-Kolmogorov or Fokker-Planck equation. Here, $V(x,t)$ is some convective flow field bacteria reside in. We may now associate a stochastic process X_t, with p as its transition density. Another way of describing the behavior is to think of it as the solution of a stochastic differential equation (SDE) which is the continuous time version of a random walk. The SDE that it satisfies can be written

$$dX_t = \sqrt{D(X_t,t)}\,dW_t + V(X_t,t)\,dt \tag{2}$$

with initial data x_0. Here, W_t is a Brownian motion. We take Eq. (2) in the Ito sense.

If we consider a higher-dimensional domain as a set of one-dimensional tubes, then this equation is generalized to

$$\frac{\partial p(t,x)}{\partial t} = \frac{1}{2}\sum \frac{\partial^2}{\partial x_i \partial x_j}[D_{ij}p(t,x)] - \sum \frac{\partial}{\partial x_i}[V_i(x,t)p], \tag{3}$$

where D_{ij} is a dispersion matrix and V_i is an advection vector. Up to this point, we have assumed that the motion of the bacteria is not confined, that is there has been no boundary effects. To study the movement in a capillary tube or microflow cell we need to augment Eqs. (3) or (5) by some boundary conditions. In the random walk, we want to impose physically meaningful boundary conditions which capture the attachment and detachment behavior of microbes. This boundary behavior is crucial in understanding the transport of microflora in porous media. In Boyd and Chakrabarty [34], the attachment/detachment process is shown to occur regularly. At each point $x \in \Gamma$ of the boundary we assign a measure of ''stickiness,'' $\rho(x)$. This measure ranges from 0, reflecting, through infinity, at which point a microbe is sorbed to the surface irreversibly. A similar model has been proposed for the flow of a chemical pushed by an inert gas through a tube with liquid state on the boundary [35]. On a domain E, with a boundary Γ, the stochastic differential equations representing the motion of a sticky bacteria are given by

$$dK_t = 1_\Gamma(X_t)\,dK_t, X_0 = x, X_t \in E, \tag{4a}$$

$$\langle N^i, N^i \rangle = \left(t - \int_0^t \rho(X_s)\,dK_s \right), \tag{4b}$$

$$dX_t = \sqrt{D}(X_t)\,dN_t + V(X_t)[dt - \rho(X_t)\,dK_t] + \gamma(X_t)\,dK_t, \tag{4c}$$

where X_t is the microbe's position, $1_\Gamma = 1$ if x is on Γ (microbe in sorbed phase) and $1_\Gamma = 0$ otherwise (microbe in aqueous phase), K_t is a measure of the time the bacteria is near to, but not on the boundary. N_t is a random directional motion which only changes when X_t is not on the boundary, γ is a directional vector which keeps the microbe inside the domain, and the bracket process $\langle N,N \rangle$ is a measure of the amount of time a particle has spent inside the domain up to time t. With these interpretations, Eq. (4a) says that K_t only increases when X_t is near (at) the boundary and the last equation states that inside the domain X_t acts as a classical Brownian motion. In this model, the rate of sorption and desorption happen relatively quickly and what is important is the ratio of the rates of sorption when the microbe is near the boundary and attachment time once on the boundary. This assumption, while rather restrictive, leads to numerical schemes which have the appropriate limiting behavior for fast reactions, and which can themselves be modified in case of slower reactions. Moreover, in the above mathematical model, the ''local time'' satisfies the equation

$$K_t = \int_0^t 1_{0 < d(X(s),\Gamma) < \epsilon}(s)\,ds, \tag{5}$$

where $d(X(s),\Gamma)$ is the distance from X to the boundary.

A. Reversible sorption

For reversible sorption, it is assumed that the expected time on the boundary and its variance are both finite. A typical assumption is that the time at the boundary is exponentially distributed. If the time on the boundary does not have finite mean and variance, the boundary behavior corresponds to deposition and a scale up or homogenization would lead to transport with decay. The appropriate boundary conditions for the Fokker-Planck Eq. (1) are known in one dimension (see Borodin and Salminen [36]) and can be immediately extended to more dimensions. Equation (1) can be rewritten as

$$\frac{\partial p(t,x)}{\partial t} = Lp(t,x), \tag{6}$$

where L is a linear operator. We require that at the boundary $p(t,x)$ satisfies

$$\frac{\partial p}{\partial n} + \rho \frac{\partial p}{\partial t} = 0, \tag{7}$$

where $\partial p/\partial n$ is the normal derivative of p and the value of $\rho \partial p/\partial t$ is taken to be the limit as one approaches the boundary from inside. This is a form of mass balance. Since no concentration is permanently sorbed, the outflow at the boundary $\partial p/\partial n$ is determined by the loss with respect to time of the concentration near the boundary $\rho \partial p/\partial t$. The usual no flow conditions correspond to $\rho = 0$, which says nothing is even temporarily stored at the boundary.

Formally, we can also write Eq. (7) as

$$\frac{\partial p}{\partial n} + \rho L p = 0. \tag{8}$$

The Fokker-Planck equation with these boundary conditions seems not to be well studied, but there is some work for the SDE approach. One of the most fundamentally useful results concerning the sticky boundary conditions is the relationship between solutions of SDE which are the same except for the boundary stickiness. Specifically, Graham [35] showed [Theorem 1.7] that if one has two measures ρ, $\overline{\rho}$, and one is subordinate to the other, that is, one has $\rho \leqslant \overline{\rho}$, then solving the SDE for ρ immediately gives a solution for $\overline{\rho}$, but

run with a different ''clock'' or ''time change.'' More precisely, the theorem states that if (X_t, K_t, ρ) is the solution of Eq. (4) and we let $A_t = t + \int_0^t (\overline{\rho} - \rho)(X_s) dK_s$ be an increasing function with inverse A_t^{-1} then $\overline{X_t} = X_{A_t^{-1}}$ and $\overline{K_t} = K_{A_t^{-1}}$ solves the SDE for $\overline{\rho}$. A particular example is taken by letting $\rho = 0$ which is subordinate to any measure of stickiness. Practically, this means that solving the reflecting boundary condition and keeping track of the local time allows one to study the sticky boundary problem. This ''time change'' is important also from a numerical point of view in that it says to approximate the SDE with a random walk model one needs to generate a reflected random walk but with a random insertion of time when it hits the boundary. The reflecting boundary condition has been numerically studied in the case of the half plane by Lepingle [37] where an Euler scheme with a good convergence rate is given. We generalize to other domains this scheme by considering them as approximately polygonal. The distribution for the inserted time can be freely set, but necessarily depends on the time step involved due to the rapidly fluctuating behavior of a Brownian motion (the local time is not differentiable).

In particular, the complex (experimentally observed) behavior remarked upon by McCaulou *et al.* [28] can be produced if the inserted time is a mixture of a highly probable small time and a less likely large time (bimodal time distribution). This separation of two characteristic time scales might be reflected in the related characteristic length scales discussed previously. The small time scale may be associated to the micron-size diffusive layer and the large time scale may correspond to the submicron double layer forces scale. This type of behavior is homogenized at large times and using an average or expected residence time is necessary when upscaling. Another important characteristic of stickiness is that it depends on location and time so that by modeling it as depending on local chemistry one can produce a behavior for microbes which mimics active ''attachment or detachment,'' something not previously recoverable. A possible model for an initial distribution of the stickiness, as a function on the boundary, could be a random function in which a covariance structure is provided. This then gives rise to a stochastic partial differential equation for evolutive problems. The situation which first interested us was modeling of bacterial attachment through a flow chamber, the upper part of which is formed by a treated slipcover [38], and the lower by a microscope slide.

B. Irreversible sorption

Irreversible sorption or deposition is modeled by using a distribution for time at the boundary with infinite moments. One of the objectives of the experimental efforts of our group is to measure single-cell attachment and detachment, the transfer of genetic information during attachment, and to develop a probabilistic model that describes these processes in aggregated scales (Darcy scale and larger). In theory, deposition implies permanent attachment. Experimentally, a particle that does not return to the aqueous phase after attaching to a solid surface for the duration of the experiment might be considered deposited.

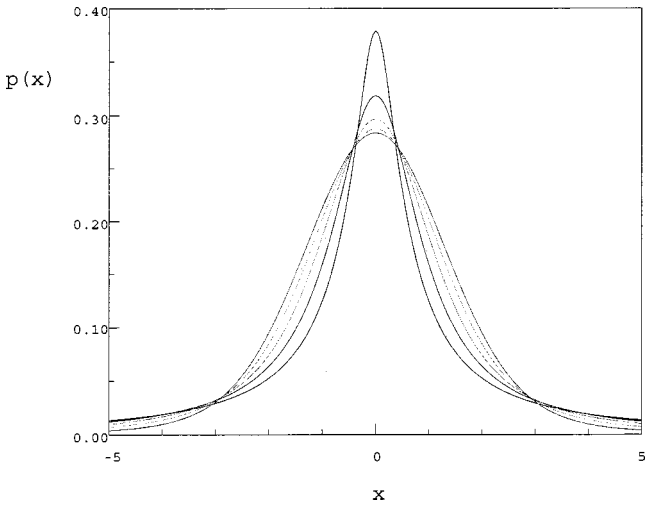

FIG. 1. Symmetric stable densities ($\sigma = 1, \beta = 0, \mu = 0$) for $\alpha = 0.75$, 1.1, 1.25, 1.50, and 1.75 (highest to lowest peak). Reproduced with the authors permission from [45].

Preliminarily, we model waiting times at the boundary as an α-stable process [39] represented by the characteristic function

$$\phi(s) = \exp(-\sigma^\alpha |s|^\alpha), \tag{9}$$

where σ and α are parameters and s is the frequency (dual to time). The inverse-Laplace transform of this characteristic function is the density. This is a particular case of an α-stable process as presented in Eq. (1). We have chosen this distribution for several reasons. Among these are: It is renormalizable and so it is easily upscaled to homogenized porous systems; it can have either finite of infinite moments (depending on α); it has heavy tails consistent with experiment; and in special cases it can mimic the common exponential distribution. Figure 1 shows a set of distributions with characteristic function (9) for different values of α and $\sigma = 1.0$. As α decreases, extreme events have higher probability. Consequently, in Fig. 1 the area under the curves in this interval $[-5,5]$ decreases with α and corresponds to heavier tails of the curves. Heavy-tailed (also referred as power-law) distributions have found physically meaning applications in multiple disciplines [40] including material fatigue, network traffic, finance, signal processing, and geosciences. The physical motivation is an observation of a process in which scales involved vary on several orders of magnitude as we have described is the case for sorption of bacteria in porous media. There exist observations and modeling of sorption with heavy-tail distributions. Drazer *et al.* [41] and Drazer and Zanette [42] conducted a series of experiments in which power-law trapping times explained observed ion transport in activated carbon porous samples. Vlad *et al.* [43] presented a thermodynamical theory consistent with Drazer's [41] observations. While research on bacteria sorption is not developed enough to provide a full description of processes, physical and chemical heterogeneities suggest that power-law scaling for long times is a reasonable assumption. The dynamical description we present explains observed long-

tailed macroscopic behavior ([44] and references therein) and provides motivation and ideas to devise pore scale experiments.

III. NUMERICAL CONSIDERATIONS

Here we discuss how random walk models are implemented in the presence of sticky boundaries. In the homogenized version where the boundaries are not visible, this is essentially a convection-diffusion-reaction (CDR) equation. Traditionally, this is solved by a particle-tracking scheme which in each instant calculates probabilities of sorption or desorption, measures the amount of time (random) in each phase (sorbed or desorbed), and then performs the random walk only on that portion of time in the desorbed phase. For fast reactions, the constant generation of random variables (for small time steps) becomes prohibitive and it is common to assume that on any fraction of time a fixed proportion is spent in either phase and then perform a random walk on the relative portion in the desorbed phase. Unfortunately, this has the unwanted effect of numerically retarding the flow, that is, changing its clock. A more uniform approach suggested by the above analysis of sticky diffusion as a basis for CDR suggests not only should a random displacement take place at each step, but also a random amount of time should be inserted into the clock.

There is not a lot of work for random walks with nonabsorbent boundaries in general and the added condition of wanting to keep track of the local time for a reflecting boundary (to be used for the random time insertion) leaves even fewer. In a paper of Lepingle's [37], an Euler scheme for reflected SDE is proposed which is not based on projecting an escaped particle back into a domain, but it is instead based on generating a random variable with the same distribution as the local time of the process and using these extra variables to keep the process inside according to Eqs. (5) and (4c) above.

The basic scheme of approximating the reflecting SDE on $(0, \infty)$ with a continuous random walk, is

$$dX_t = \sqrt{D}(X_t)dW_t + V(X_t)dt + dK_t, \quad X_t \in (0,\infty) \quad (10)$$

or in a half space

$$X_0 = x_0, \tag{11a}$$

$$Y_{t+\Delta t} = V(X_t)\Delta t + \sqrt{D}(X_t)W_{\Delta t}, \tag{11b}$$

$$K_{t+\Delta t} = K_t + \max\left(0, -X_t + \frac{\sqrt{D(X_t)^2 Z + Y_t^2} - Y_t}{2}\right), \tag{11c}$$

$$X_{t+\Delta t} = X_t + Y_{t+\Delta t} + \gamma(K_{t+\Delta t} - K_t). \tag{11d}$$

Here, $W_{\Delta t}$ is a Gaussian random variable with mean zero and variance Δt and Z is distributed as an exponential with mean $2\Delta t$. The reason that this scheme approximates correctly a reflected diffusion is that reflection in a line is a simple matter of taking any continuous function and adding another function which together always stays positive [37]. This so-called Skorohod problem in the case of a random walk Brownian motion is determined by the infimum of the process which in turn is given as an exponential random variable of the type discussed. In a half space, each component has a covariance matrix for the dispersion, but this does not change the scheme much. A way of simulating flow through a two-dimensional tube with reflecting boundaries is to make the time step small enough so that one cannot during that interval hit both boundaries, then treat the problem only locally, that is, one can keep track of a separate local time at each boundary and adjust the random walk accordingly. An obvious problem with this scheme is that it cannot be readily extended to other types of bounded domains in two dimensions, much less to a circular capillary in three dimensions. This however is not a problem here as we are working in a slit domain.

The simulation of a sticky process follows the above scheme except that the sets of points making up the trajectories for one realization (t, X_t) are replaced with $[t + \int_0^t \rho(X_s)dK_s, X_s]$. If one is interested in the position of a particle at a particular time τ it can be had by finding the time t for which $A_t = \tau$. One usually knows in advance the times of interest and can simply calculate the time t when it first surpasses τ. First passage times are especially easy since one knows the position the particle is at when the time is reached and hence one need only keep track of A_t.

An alternative to this approach is "time marching" that uses a strict discretization of time to construct a simple random walk. Upon hitting the boundary, the particle sticks and then desorbs from the boundary with a probability say ϵ. However, to capture the boundary behavior of continuous diffusions (which have infinite variation) with a discrete process requires a dependence of ϵ on the time step. We show in Appendix B that the appropriate order for ϵ takes the form of

$$\frac{\epsilon}{(1+\epsilon)^2} = \frac{\rho}{\sqrt{\Delta t}}. \tag{12}$$

A disadvantage is that as $\Delta t \to 0$, $\epsilon \to 1$, so that a large effort is made in calculating almost certain events. Moreover, it is well known that a Poisson random variable is the limit of appropriately scaled binomial random variables and so the first exit from a wall is given by the distribution of the (inter)arrival times of a Poisson which has an exponentially decaying distribution. This means that upon averaging, the two approaches are equivalent.

In passing, we make a few comments for circular capillaries. For a circular domain with no drift one can write the Laplacian in polar coordinates, that is, the rectangular Lagrangian process X_t, Y_t can be thought of as the product of a radial process R_t and angular process Θ_t. This corresponds to a skew product decomposition of Brownian motion where the radial process satisfies the stochastic differential equation

$$dR_t = \frac{1}{2R_t}dt + dW_t \tag{13}$$

together with reflection on the boundary. While the angular process of interest satisfies

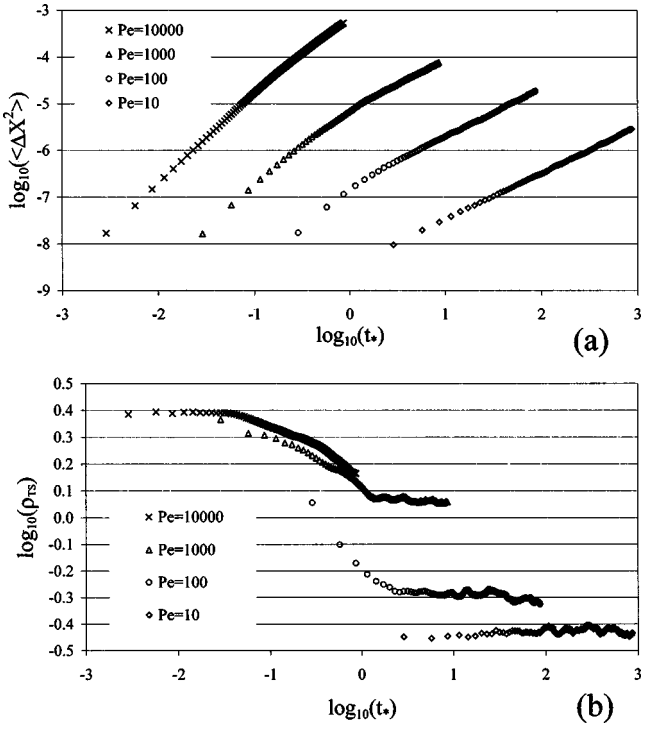

FIG. 2. Mean-square displacement $\langle \Delta X^2 \rangle$ (m^2) and ρ_{TS} for sorptive time with exponential distribution with parameter $\lambda = 0.5$ and various values of Péclet number $\mathrm{Pe} = vb/D_0$.

$$3d\Theta_t = \frac{1}{R_t^2} dB_t, \quad (\mathrm{mod}\ 2\pi), \tag{14}$$

where W_t is a Brownian motion on the line (one-dimensional random walk), and B_t is a Brownian motion on the unit circle. One can now apply Lepingle's ideas to the radial process without much trouble. The angular process can be thought of as taking place on the real number line and then mapped onto the circle. The coefficient of its dispersion, $1/R_t^2$, can be integrated approximately by taking the average of $1/R_t^2$ and $1/R_{t+\Delta t}^2$.

In more complicated polygonal-like domains, one can perform a decomposition of the domain into overlapping wedges (cones), keep track of the particles position relative to the decomposition and near the boundary reflect the angular part alone.

A discussion of the α-stable deviate generator can be found in Appendix A.

IV. RESULTS

As a reference, and in order to check the correctness of the procedure and algorithms, we tested the case of Taylor dispersion in a reflecting slit capillary (Brenner and Edwards [46]) with known asymptotic solution for the mean-square displacement

$$\langle \Delta X^2 \rangle_{\mathrm{Taylor}} = \begin{cases} 2D_0 t + \dfrac{1}{2} v^2 t^2 + O(t^3) & \text{if } t \ll b^2/D_0 \\ \left(2D_0 + \dfrac{v^2 b^2}{\pi^2 D_0} \right) t + O(t) & \text{if } t \gg b^2/D_0, \end{cases} \tag{15}$$

where v denotes the cross-sectional average velocity, D_0 is the diffusive (motility) coefficient, and b is the half width separation between walls. The mean-square displacement $\langle \Delta X^2 \rangle$ is computed as

$$\langle \Delta X^2 \rangle = \langle X^2 \rangle - \langle X \rangle^2, \tag{16}$$

where the first moment $\langle X \rangle = vt$. The numerical algorithm produced Taylor dispersion with relative errors under 1%.

The two main parameters controlling the dynamics of the problem are the time $t_b = b^2/D_0$ referred hereafter as the cross-channel motility time, and the ratio of convective to motility fluxes which is called the Peclet number $\mathrm{Pe} = vb/D_0$. We define the dimensionless time $t_* = t/t_b$, the average time spent in the aqueous phase t_a, the total simulation time t_m, and the average time spent in the sorbed phase $t_s = t_m - t_a$ and let $\rho_{\mathrm{TS}} = \langle \Delta X^2 \rangle_{\mathrm{Taylor}} / \langle \Delta X^2 \rangle_{\mathrm{sim}}$. We compare the mean-square displacement of Taylor dispersion [Eq. (15)], $\langle \Delta X^2 \rangle_{\mathrm{Taylor}}$, to the mean-square displacement with sorption (exponential or α-stable waiting times as indicated) $\langle \Delta X^2 \rangle_{\mathrm{sim}}$. If we consider long times $t_* \gg 1$, then $\langle \Delta X^2 \rangle_{\mathrm{Taylor}} = D_{\mathrm{eff}} t_*$ and $\langle \Delta X^2 \rangle_{\mathrm{sim}} = D_{\mathrm{eff}}^* t_*^{\gamma}$ and $\rho_{\mathrm{TS}} = D_{\mathrm{eff}} / D_{\mathrm{eff}} t_*^{1-\gamma}$. In a $\log_{10}$-$\log_{10}$ plot ρ_{TS} versus t_* the slope is $1-\gamma$ and the intercept with the axis $t_* = 0$ is $\log_{10}(D_{\mathrm{eff}}/D_{\mathrm{eff}}^*)$ (slope and intercept of a tangent at any t_*). If the slope of this curve is positive then we call the event subdispersive ($\gamma < 1$) and if it is negative we call it superdispersive ($\gamma > 1$). If the intercept with the t_* axis is negative we have $D_{\mathrm{eff}} < D_{\mathrm{eff}}^*$, although this is only a relevant comparison for $\gamma \approx 1$.

Next, we analyze an exponential waiting time for which the solution is known. If X has an exponential distribution with parameter λ, then its density is $f(x) = \lambda \exp(-\lambda x)$ and its expected value is $1/\lambda$. Here, the same relationship (15) applies with reduced velocity $v_r = v/R_0$ and reduced diffusion coefficient $D_r = D_0/R_0$, where R_0 is a constant known as the retardation factor. Figure 2 gives $\langle \Delta X^2 \rangle$ and ρ_{TS} for $\lambda = 0.5$, velocity $v = 10^{-5}$ m/s and width $b = 10^{-5}$ m and varying diffusion coefficient D_0 (this implies both t_b and Pe change). For short times ($t_* < 2$) subdispersion is observed ($\gamma < 1$) that converges to Taylor dispersion when $t_* > 2$ as we expect. After Taylor dispersion is established, the time scaling of the mean-square displacement is linear $\gamma = 1$, yet the effective dispersion D_{eff}^* depends on D_0, which dictates the collision frequency of the particles with the walls.

A. α-stable waiting times

We examine the effects of an α-stable waiting time distribution on transport as a function of the parameters $t_b = b^2/D_0$ and $\mathrm{Pe} = vb/D_0$. Both α and σ control the sorption process. We set $\sigma = 1$ and focus on α (Table I) which describes the frequency and magnitude of extreme events (represented by the heaviness of the tail of the distribution) of times spent at the boundary. A large number of particles ($N = 5000$) were released uniformly from a line transverse to the main direction of flow. To understand the dynamics, let us summarize some basic results of the simulations. The scaling in time of mean position and mean average displace-

TABLE I. Parameter range investigated.

Parameter	Values	Units
v	10^{-6}, 4.0×10^{-6}, 1.6×10^{-5}, 6.4×10^{-5}, 2.56×10^{-4}	m/s
D_0	10^{-14}, 10^{-13}, 10^{-12}, 10^{-11}	m^2/s
b	10^{-5}, 4.0×10^{-5}, 1.6×10^{-4}, 6.4×10^{-4}	m
α	0.4, 0.8, 1.2, 1.6, 2.0	dimensionless

ment is key to understand transport. Closely related to this scaling is the average number of collisions with the wall N_c that as we will see shortly depends on t_b yet it is velocity invariant.

For fixed total simulation time t_m, we study the dependence of t_a (average time in aqueous phase) and t_s (average time in sorbed phase) on α and t_b. Figure 3(a) shows t_a/t_m and t_s/t_m for $t_m=86\,400$ s (one day). In Figs. 3(b)–3(d), extreme events have been identified by separating the average time in the sorbed phase into nonextreme events defined by time t_{s1}, and extreme events defined by t_{s2} such that $t_s=t_{s1}+t_{s2}$. An extreme sorption event of duration t_e is defined to be when $t_e>t_f$ where t_f is a cutoff time. Various cutoffs used are presented in Table II. Details of the separation of t_s into nonextreme and extreme events are given in Appendix C. One can think of a combination of reversible (quantified by t_{s1}) and irreversible (t_{s2}) events taking place. For the same bacterial motility relative to the pore size, that is, for a fixed value of t_b, bacteria will spend a greater fraction of time in the aqueous phase with greater α. Smaller values of α induce both a greater range of sorbed times and longer sorption times upon collision against a surface and this agrees with the behavior of α-stable distributions.

Comparing the ratio t_a/t_m as a function of t_b between α-stable [Fig. 3(a)] and an exponential (not shown) it is found that both are diffusive in shape. To illustrate how extreme events influence this behavior, Fig. 3(b) shows the ratio between average time in the aqueous phase and the sum t_a+t_{s1}. Figure 3(c) is a plot of $(t_a+t_{s1})/t_m$ versus t_b. When this fraction is zero (as a function of α and t_b) we are in a deposition regime. When $\alpha<0.5$, complete deposition is possible and it occurs for low values of t_b; e.g., for $\alpha=0.4$, deposition occurs for $t_b<100$. For $\alpha>0.5$, total deposition does not occur [$(t_a+t_{s1})/t_m$ never reaches zero]. Figure 3(d) shows the fraction of the simulation time these extreme events take, t_{s2}/t_m, as a function of t_b. If the cross-channel relative motility of the bacteria $1/t_b\equiv D_0/b^2$ is small enough (or correspondingly the characteristic cross-channel motility time $t_b=b^2/D_0$ is large enough), collision frequency is low and sorption is limited. Consequently, a larger fraction of time is spent in the aqueous phase. For large relative motility, D_0/b^2, $t_{s2}^{(m)}$ becomes a constant [plateau to the left of the t_b axis in Fig. 3(d)]. The constant is the fraction of simu-

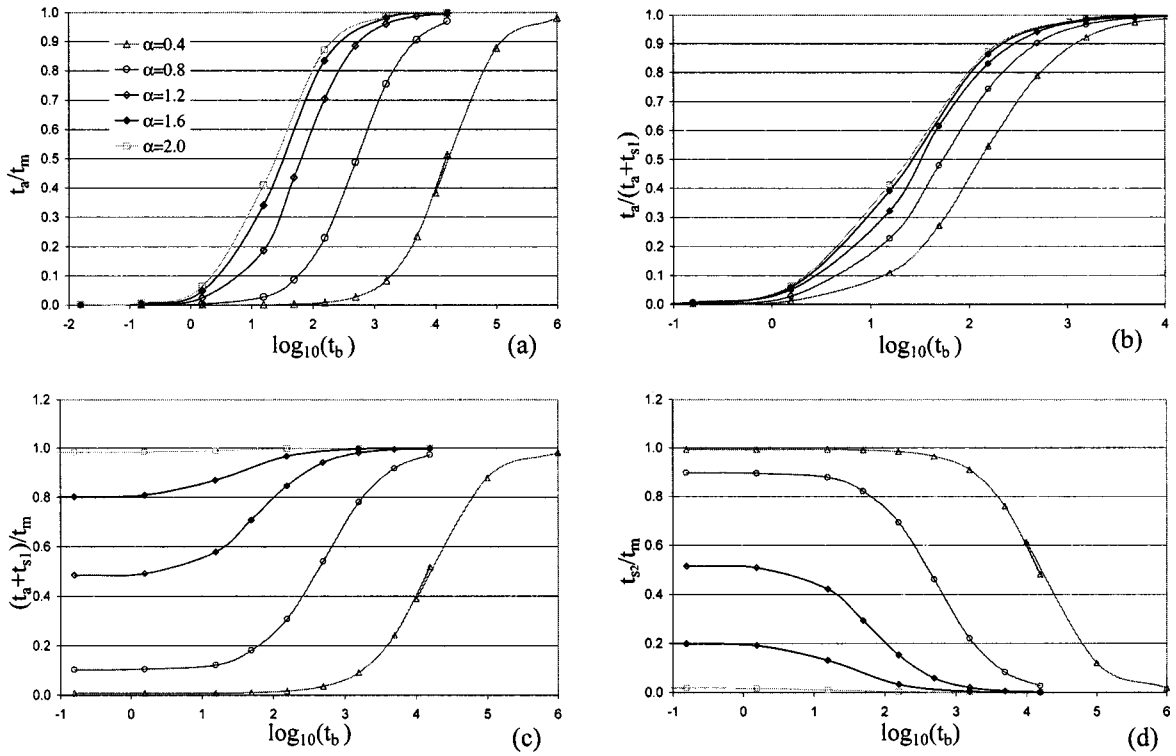

FIG. 3. Average time in aqueous (t_a) and sorbed (t_s) phase after $t_m=86\,400$ s. t_b in seconds (s).

TABLE II. Cutoff values for extreme sorbed times.

α	0.4	0.8	1.2	1.6	2.0
t_f cutoff	120.18	33.65	13.215	6.653	4.021
$P(\|T\| \leq t_f)$	0.90	0.96	0.975	0.9975	0.999

lation time bacteria stick to the boundary due to events of duration greater than the cutoffs in Table II. This fraction, tabulated in Table III, depends on both α, and the selected cutoff t_f. These values illustrate how deposition increases as the value of α decreases. For instance, for $\alpha=0.8$ [second curve from right to left in Fig. 3(d)], a few long-time (strong) sorption events account for nearly 90% of the simulation time while for $\alpha=1.2$ these extreme events that may represent deposition account for only 50% of the simulation time.

Figure 4 shows the average number of collisions, N_c, as a function of t_b. The average number of collisions dictates the probability of attaching to a surface. Small t_b (high-relative motility) gives rise to collision saturation. The saturation (plateau) occurs at a critical motility for which any additional energy invested by the bacteria for motility does not accelerate sorption kinetics

Three transport or sorption regimes are apparent in Fig. 4:

(1) High-motility (small t_b) regime: Frequent collisions will cause sorption kinetics to be fast, that is, equilibrium will be approached quickly. Depending on the value of α, this means rapid deposition ($\alpha<1$) or a decrease in the time fraction in the aqueous phase ($\alpha>1$).

(2) Low-motility (large t_b) regime: Slow sorption kinetics and greater time is spent in the aqueous phase.

(3) Transition regime: The transition between the two regimes is shaped similar to a diffusion front.

The mean number of particles in the aqueous phase, $\langle K_a \rangle$, is a kinetic quantity. This kinetic parameter is ignored when looking at time averages as in Fig. 3(b). We study the time dependence of $\langle K_a \rangle$ and $\langle K_s \rangle$ ($N_p=\langle K_a \rangle+\langle K_s \rangle$) in Fig. 5. Figures 5(a)–5(d) show the evolution in time of the concentrations in the aqueous and sorbed phases for selected values of t_b and different values of α with $t_m=24$ h. The value of t_b for these plots was selected so that $C_a=\langle K_a \rangle/N_p$ is close to 0.5. Figure 5(a) corresponds to $\alpha=0.4$ and $t_b=1.56\times10^4$. According to Table II, about one in ten collisions has a sticking time greater than two minutes ($t_f=120$ s). Yet it can be seen that after $t_m=24$ h equilibrium has not been reached and bacteria are still slowly depositing on the walls. This is an example of slow kinetic sorption where most events of reversible sorption last under two minutes, yet rare deposition events dominate the long-term kinetics. From Figs. 5(a)–5(d) and other simulations, it is possible to conclude that the resulting regimes include both irreversible deposition and reversible sorption. If $\alpha<1$ deposition occurs. As $\alpha\uparrow1$ the deposition occurs in a slower fashion [Figs. 5(a), 5(b); Fig. 5(b) corresponds to $\alpha=0.8$ and $t_b=4.94\times10^2$]. For $\alpha>1$, reversible sorption takes place. As α increases above one, the kinetic effects have shorter duration and equilibrium between sorbed and aqueous phases is reached quickly [Figs. 5(c), where $\alpha=1.2$ and $t_b=49.4$, and 5(d) where $\alpha=1.6$ and $t_b=15.6$].

TABLE III. Fraction of extreme sorption events to simulation time, for high-relative cell motility.

α	0.4	0.8	1.2	1.6	2.0
t_f cutoff	120.18	33.65	13.215	6.653	4.021
$\max t_{s2}^{(m)}$	0.993	0.897	0.515	0.199	0.0175

B. Moments

The number of collisions, mean number of particles in the aqueous and sorbed phases, and mean time spent in each phase are dependent only on the parameters α and t_b and independent of the mean velocity v. This is in contrast with both the mean position and mean-square displacement which are velocity dependent. The average position of an ensemble of 2000 particles is shown in Fig. 6(a) for the same values of α and t_b used in Figs. 5(a)–5(d). Figure 6(b) gives the flow retardation $R_0=\langle X \rangle_v/\langle X \rangle_{\rm sim}=v t_*/V_{\rm eff}^* t_*^\theta$ which is the ratio between the mean displacement of a nonsorptive species with average velocity v to that of a simulated sorptive species. Retardation converges to a constant value only for $\alpha>1$.

Figures 7(a)–7(b) show the mean-square displacement and $\rho_{\rm TS}$ for the same selected values of α and t_b as in the previous two plots. The reader should note that the mean-square displacement is defined by $\langle \Delta X^2 \rangle=\langle [X(t)-\langle X(t) \rangle]^2 \rangle$ where in general $\langle X(t) \rangle \neq vt$ with v the mean velocity. We call $\langle \Delta X^2 \rangle$ superdispersive if it scales with t^γ where $\gamma>1$, Taylor dispersive if $\gamma=1$, and subdispersive otherwise. It should be noted that this terminology applies when talking about the rate of growth in time (proportional to γ for any given time) yet the total mean-square displacement for a superdispersive situation may still be bound by Taylor dispersive mean-square displacement, that is, $\langle \Delta X^2 \rangle_{\rm super}=D_{\rm eff}^* t^\gamma<D_{\rm eff} t=\langle \Delta X^2 \rangle_{\rm Taylor}$ is possible with $\gamma>1$. For $\alpha=2.0$, dispersion scales as Taylor [Eq. (15)] while $\alpha<2.0$ are superdispersive. As pointed out earlier, when $\alpha<1$, slow deposition regimes develop and are noticeable for $t_*\gg1$. This renders $t_m=1$ day insufficient to observe long-time dispersive effects, so we set $t_m=100$ days$=8.64\times10^6$ s for the smaller values of α. Figures 8(a) and 8(c)

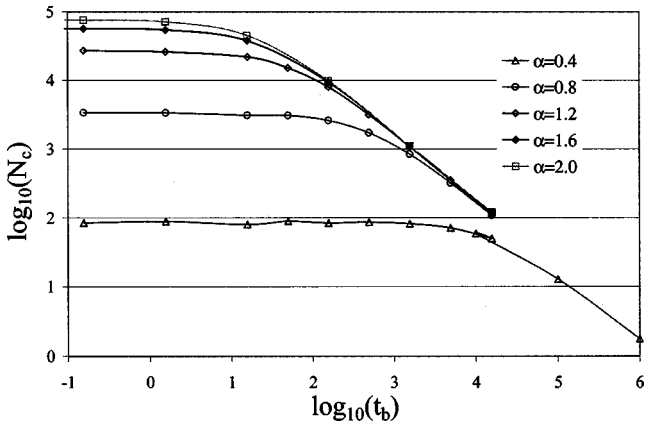

FIG. 4. Number of collisions N_c for various values of α after $t_m=86\,400$ s of total simulation time. t_b in seconds (s).

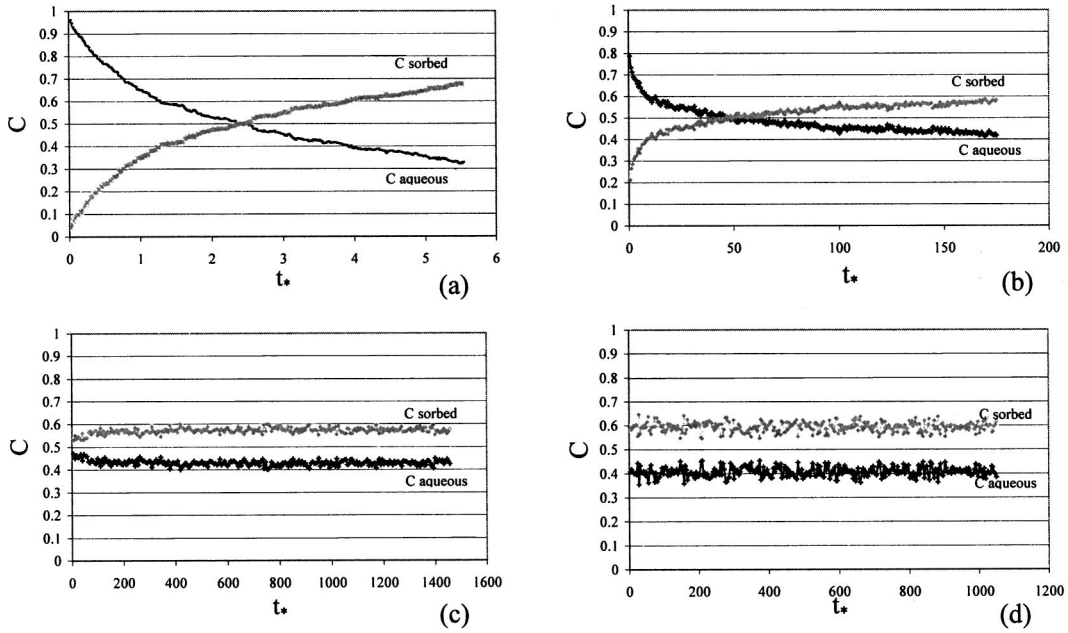

FIG. 5. Concentration in the aqueous and sorbed phases (C_a and C_s) for various values of α after $t_m=1$ day. (a) $\alpha=0.4$; (b) $\alpha=0.8$; (c) $\alpha=1.2$; and (d) $\alpha=2.0$. C, t_* are dimensionless.

show the mean position and mean-square displacement for these longer simulations. Figures 8(b) and 8(d) gives the retardation factor R_0 and ρ_{TS}. On a $\log_{10}$-$\log_{10}$ scale, the dependence of $\langle X\rangle$ and $\langle \Delta X^2\rangle$ on $t_*=t/t_b$ appears linear when $t_*>10$. Small t_* corresponds to a lower total number of wall collisions (slow sorption kinetics) and therefore it is expected to transition between a ''pure'' (no sorption) Taylor dispersion ($t_*<10$) to apparent anomalous dispersion ($t_*>10$) resulting from sorption.

We posit $\langle X\rangle=V_{\mathrm{eff}}^* t_*^{\theta}$ and perform regressions to estimate V_{eff}^* and θ. Figure 9(a) shows θ for $\alpha=0.6$ (top curve) and $\alpha=0.4$ (bottom curve). The ($\log_{10}$ of) coefficient V_{eff}^* is

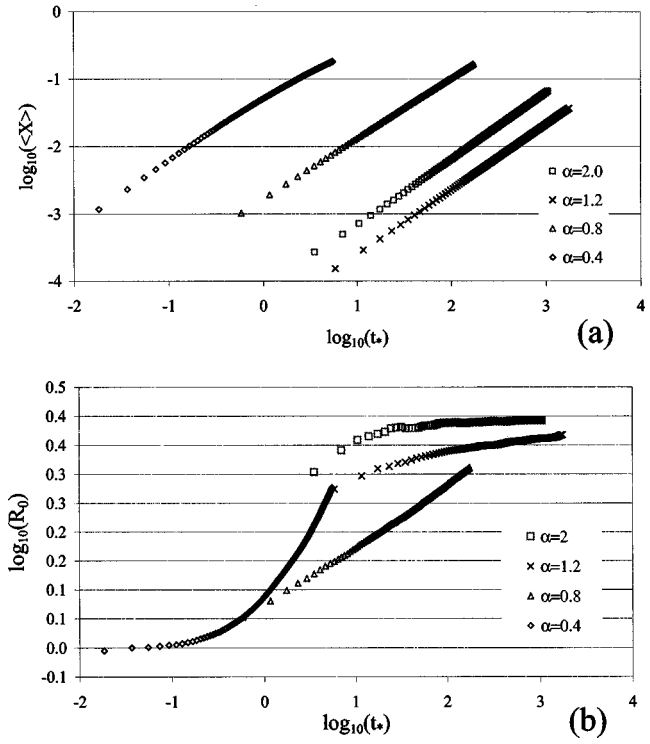

FIG. 6. (a) Mean particle position and (b) retardation factor R_0 for selected values of α and t_b after $t_m=1$ day of total simulation time. $\langle X\rangle$ in meters (m), R_0 and t_* are dimensionless.

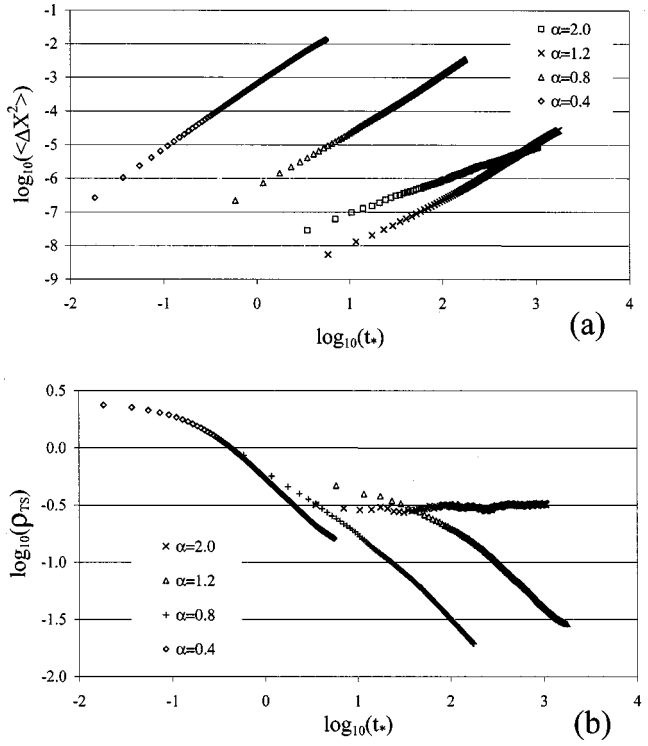

FIG. 7. (a) Mean particle dispersion and (b) ρ_{TS} for selected values of α and t_b after $t_m=1$ day of total simulation time. $\langle \Delta X^2\rangle$ in (m^2), ρ_{TS} and t_* are dimensionless.

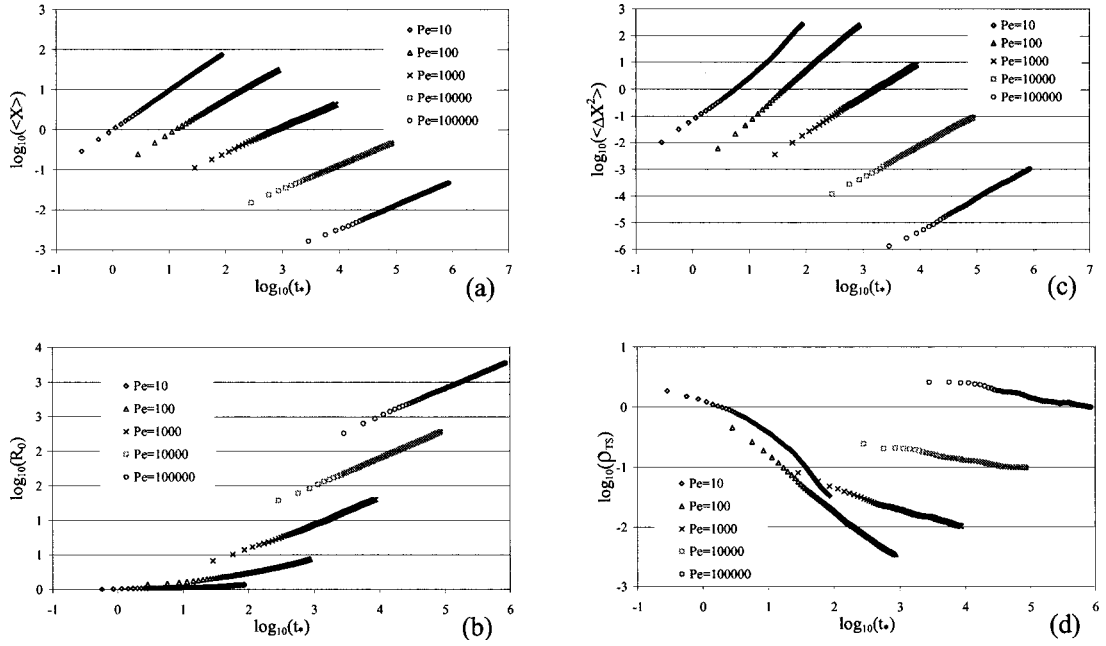

FIG. 8. (a) Mean position; (b) retardation factor; (c) mean-square displacement; and (d) ρ_{TS} for $\alpha=0.6$ after $t_m=100$ days of total simulation time. Different curves correspond to different values of Péclet number as marked. $\langle X\rangle$ in meters (m), ΔX^2 in (m^2).

shown in Fig. 9(b) for both values of $\alpha=0.4$ and $\alpha=0.6$. Below a threshold $t_b<T_{xa}$, $\theta=\alpha$ (here, T_{xa} depends on α). For $t_b>T_{xa}$, $\theta\rightarrow 1$ and the mean displacement appears linear. V^*_{eff} is not to be confused with the effective velocity, as it is clearly larger than the maximum velocity. The true effective velocity is $V_{\mathrm{eff}}=V^*_{\mathrm{eff}}t_b^{\theta-1}$ and it is always bounded by the maximum fluid velocity.

For the mean-square displacement, we also posit $\langle\Delta X^2\rangle=D^*_{\mathrm{eff}}t_*^{\gamma}$ Figures 9(c) and 9(d) show γ and D^*_{eff} for $\alpha=0.6$ [circles in Fig. 9(d)] and $\alpha=0.4$ [triangles in Fig. 9(d)]. For $\alpha=0.6$, the regime appears superdispersive ($\gamma>1$) and evolves from $\gamma=2\alpha$ towards $\gamma=2$ as t_b increases. For $\alpha=0.4$, the regime appears subdispersive for $t_b<T_{xa}$ and then as γ increases it appears superdispersive. D^*_{eff} increases with

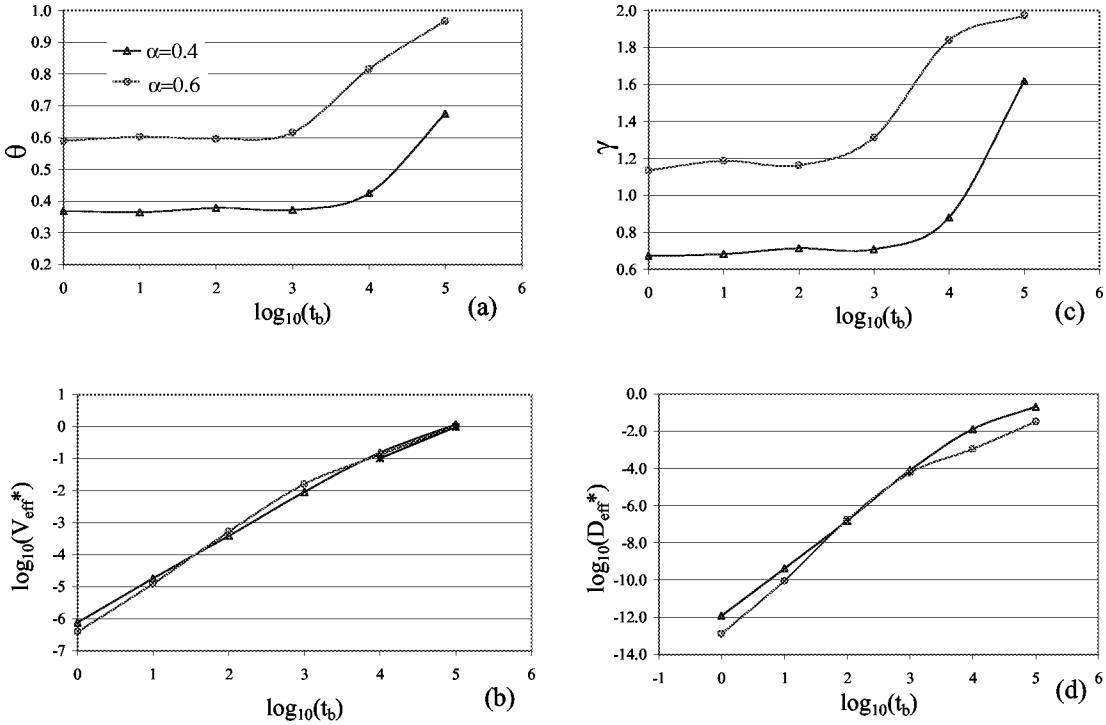

FIG. 9. Coefficients in fractional regressions for mean position $\langle X\rangle=V^*_{\mathrm{eff}}t_*^{\theta}$ and mean-square displacement $\langle\Delta x^2\rangle=D^*_{\mathrm{eff}}t_*^{\gamma}$ as functions of t_b and α. (a) θ for $\alpha=0.4$ (upper curve) and $\alpha=0.6$ (lower curve), (b) V^*_{eff} for $\alpha=0.4$ (triangles) and $\alpha=0.6$ (circles), (c) γ for $\alpha=0.4$ (upper curve) and $\alpha=0.6$ (lower curve), and (d) D^*_{eff} for $\alpha=0.4$ (triangles) and $\alpha=0.6$ (circles). t_b in seconds (s).

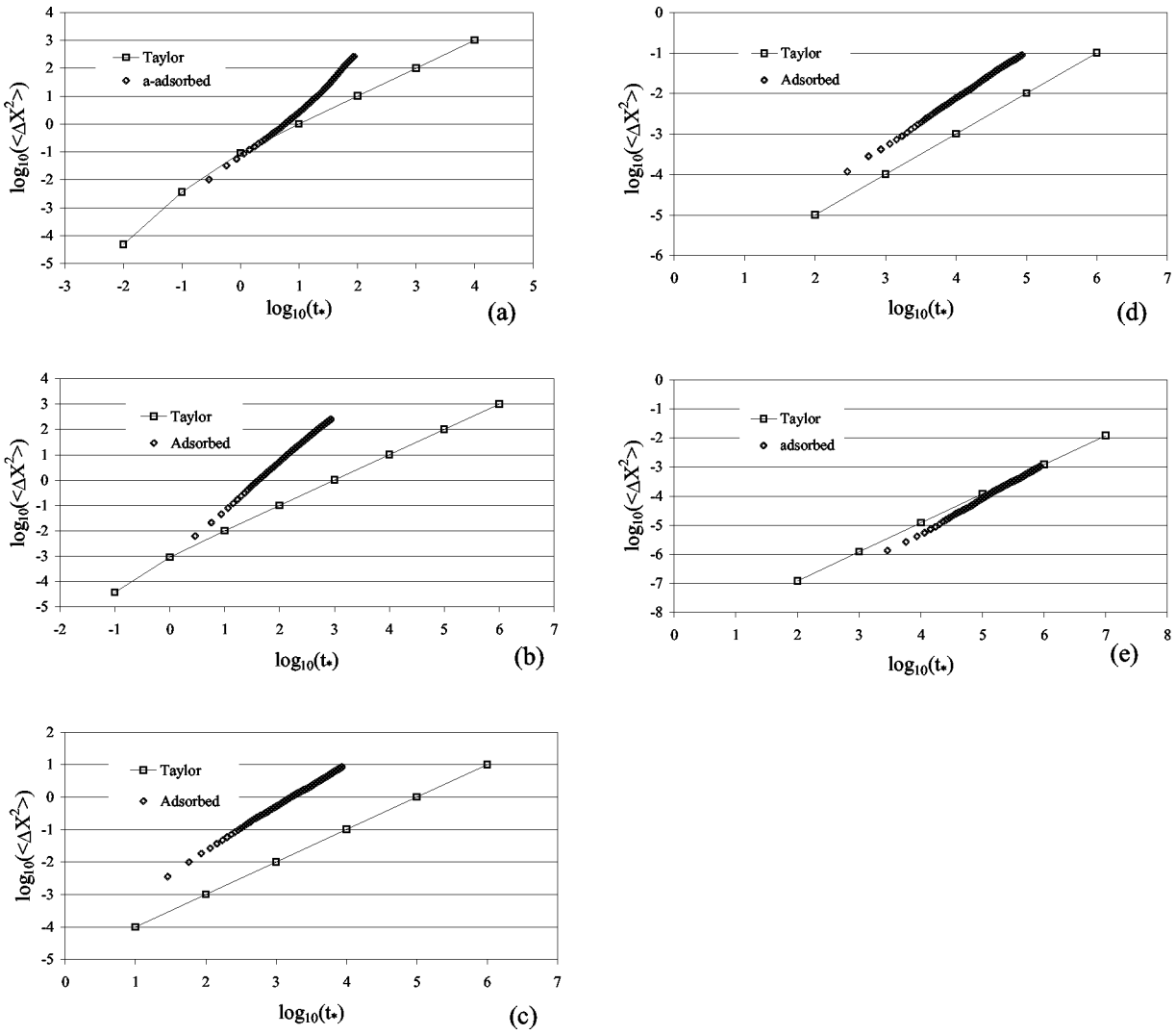

FIG. 10. Comparison of the Taylor dispersion of a nonsorbing species (labeled Taylor) and the dispersion of an α-stable sorbing bacteria for $\alpha=0.6$. Different curves correspond to different values of t_b: (a) $t_b=10^5$; (b) $t_b=10^4$; (c) $t_b=10^3$; (d) $t_b=10^2$; and (e) $t_b=10$. $\langle \Delta X^2 \rangle$ in (m^2), t_* is dimensionless.

t_b and does not depend on α. Since γ increases monotonically as well, we draw the conclusion that α-stable sorption enhances dispersion by several orders of magnitude (relative to Taylor dispersion of a nonsorptive species) for values of $\alpha>0.5$. Maximal dispersion occurs for the greater values of t_b. Figures 10(a)–10(e) compare Taylor dispersion of a nonsorbing to an α-stable sorbing species with $\alpha=0.6$ Figure 10(a) exhibits a distinct behavior for early times $t_*<6$ very close to Taylor dispersion and then transitions to apparent superdispersion. This can be explained by noting that the sorbing boundary creates retardation after sufficient time and consequently enhances dispersion. For $t_b=10^5$, collisions are infrequent and this effect is observable at the time scale analyzed in the simulations presented. For values of $t_b<10^5$, we observe a well-established long-time regime for both the nonsorptive and sorptive cases. We conclude that our analysis is centered on long-term dispersion for the sorptive case and it is characterized by retardation in the mean position and superdispersion.

We next analyze the sensitivity of estimation in the parameters θ, V^*_{eff}, γ, and D^*_{eff} and further elucidate on our discussion of short versus long-term dispersion. The goodness of fit parameter for all regressions is $R^2>0.99$. Figure 10(a) shows $\langle \Delta X^2 \rangle$ for $\alpha=0.6$ and $t_b=10^5$. It suggests that short time $t_*<6$ behavior may not be described accurately by the fractional law with $D^*_{\text{eff}}=3.33\times10^{-2}$ and $\gamma=1.97$, even if $R^2=0.994$. We separate short-and long-time moments and estimate parameters in each subrange. For $t_b=10^5$, the short-time range corresponds to $t_*<6$. An analogous procedure is employed for the selection of the threshold for other values of t_b.

Figures 11(a)–11(d) display the coefficients in $\langle \Delta x^2 \rangle = D^*_{\text{eff}} t_*^{\gamma}$ as a function of t_b for short times (triangles), long times (diamonds), and over the entire range (crosses) for $\alpha=0.4$ [Figs. 11(a) and 11(b)] and $\alpha=0.6$ [Figs. 11(c) and 11(d)]. For $\alpha=0.4$, γ and D^*_{eff} [Figs. 11(a) and 11(b)] behave consistently. For $t_b<10^3$, $\gamma\approx 3\alpha/2$ is constant with respect to t_b while for long times $\gamma\approx 2\alpha$. The values of γ are very

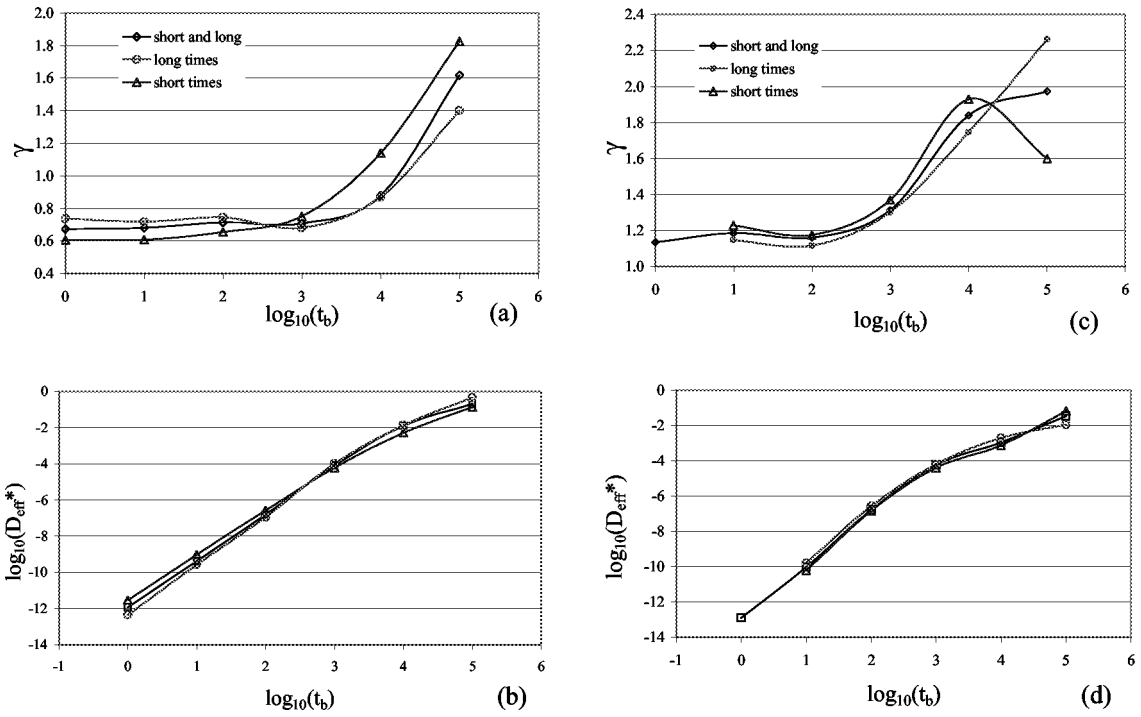

FIG. 11. Coefficients in fractional regression for mean-square displacement, $\langle \Delta x^2 \rangle = D^*_{\text{eff}} t^{\gamma}_*$, as functions of t_b and α. Estimation performed with simulation $t_m = 100$ days long considering all time range (crosses), short times (triangles), and long times (diamonds). (a) γ for $\alpha = 0.4$, (b) D^*_{eff} for $\alpha = 0.4$, (c) γ $\alpha = 0.6$, and (d) D^*_{eff} for $\alpha = 0.6$. t_b in seconds (s).

close for $t_b < 10^3$ using the short- and long-time evolution of $\langle \Delta x^2 \rangle$. For $t_b > 10^3$, apparent subdispersive behavior evolves into superdispersive spreading. The coefficient D^*_{eff} [Fig. 11(b)] remains unchanged even with the fluctuations of γ. The consistency of the estimated values for γ and D^*_{eff} suggests the scaling can be defined universally for long times.

For $\alpha = 0.6$, γ [Fig. 11(c)] behaves monotonically except at $t_b = 10^5$ for the short-time estimator where a sudden decrease in γ occurs. As we discussed previously, this is due to a change in dispersion regime which is controlled by the wall collision frequency. Since $\gamma > 1$ for all t_b, the dispersion regimes for $\alpha > 0.5$ appear superdispersive. The behavior of γ for long times is always monotonic suggesting universal scaling. The behavior of D^*_{eff} [Fig. 11(d)] is very similar to the case $\alpha = 0.4$.

C. Effect of Pe number

We consider now convective flux relative to the motility flux in the form of Péclet number, $\text{Pe} = vb/D_0$. Figure 12(a) shows $\langle \Delta X^2 \rangle_{\text{sim}}$ and Fig. 12(b) shows the benchmark ratio $\rho_{\text{TS}} = \langle \Delta X^2 \rangle_{\text{Taylor}} / \langle \Delta X^2 \rangle_{\text{sim}}$ for a simulation with $\alpha = 0.4$ and constant $t_b = 2 \times 10^4$. Figures 12(a) and 12(b) shows that both γ and D^*_{eff} depend on the Péclet number in a nonlinear fashion. Dispersion is initially Taylor scaled ($\gamma \approx 1$) for t_* < 1 for all Péclet numbers. As t_* increases, for low Péclet numbers the transport is subdispersive. As Pe increases, ($\text{Pe} \approx 0.5$) the transport turns superdispersive for small t_*, reaches a Taylor scaled plateau, and then turns subdispersive for large t_*. Physically, we know deposition is taking place ($\alpha = 0.4 < 1$) and since $t_b = 2 \times 10^4$ is constant for all curves in Fig. 12(b) we expect that for large $t_* > 10^3$, the particles will be mostly in the sorbed phase with infrequent excursions into the aqueous phase resulting in subdispersive behavior. However, while there are numerous particles in the aqueous phase, $t_* < 10^2$ they take more frequent excursions to sample the velocity field. Being the sorption times are α-stable distributed, this sampling occurs in such a fashion that the overall result is superdispersion. This corresponds well to the case of strong sorbers studied by Bychuk and Oshaughessy [47], its scaling being that of a Levy walk. As for the first moment $\langle X \rangle$, it scales like $\langle X \rangle = V^*_{\text{eff}} t^{\theta}_*$ with $\theta = \alpha$ for t_* > 100. For $t_* < 5$, it scales like flow with average velocity v and is linear in time.

We now consider the case of reversible or weaker sorption, $\alpha > 1$. In Figs. 13(a) and 13(b) $\alpha = 1.2$, $\text{Pe} < 1$. At low Pe, this results in no coherent net deterministic displacement $\langle X \rangle$ and diffusive motility dominates. We have pointed out that different sorption regimes develop with t_b. We first consider the case for small t_b. The upper curve in Fig. 13(b) is for $t_b = 0.11$, that is, the particles collide very often with the surface. This regime is diffusion dominated and therefore not very sensitive to velocity. It evolves from subdispersive ($D_{\text{eff}} < D^*_{\text{eff}}, \gamma < 1$) for small t_* to a delayed Taylor dispersive ($D_{\text{eff}} < D^*_{\text{eff}}, \gamma \approx 1$) regime for large t_*. For $t_b = 1000$, the lower-left curves in Fig. 13(b) correspond to different values of the velocity (keeping $\text{Pe} < 1$). Dispersion is Taylor scaled ($\gamma \approx 1$), yet it is a fraction (by a factor of 2) of the nonsorptive case ($D_{\text{eff}} < D^*_{\text{eff}}$). This is consistent with the fact that the particles are mostly in the aqueous phase. In conclusion, for $\alpha > 1$ and low Péclet numbers, the resulting dispersion will

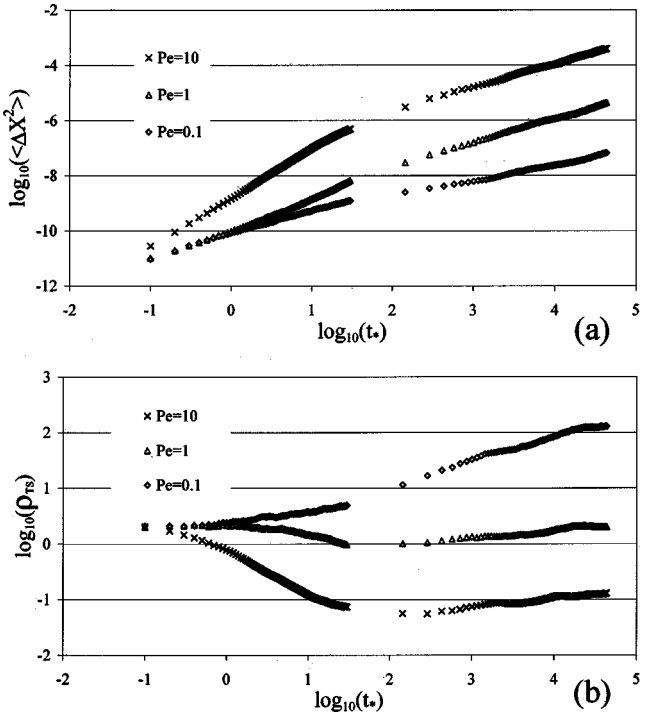

FIG. 12. Mean-square displacement $\langle \Delta x^2 \rangle_{\mathrm{sim}} = D^*_{\mathrm{eff}} t^{\gamma}_*$ variation with Péclet number $\mathrm{Pe} = v d / D_0$. Fixed $t_b = 2 \times 10^4$ and $\alpha = 0.4$. (a) $\langle \Delta x^2 \rangle_{\mathrm{sim}} = D^*_{\mathrm{eff}} t^{\gamma}_*$, (b) Benchmarking ratio against Taylor dispersion $\rho_{\mathrm{TS}} = \langle \Delta X^2 \rangle_{\mathrm{Taylor}} / \langle \Delta X^2 \rangle_{\mathrm{sim}}$. $\langle \Delta X^2 \rangle$ in (m^2).

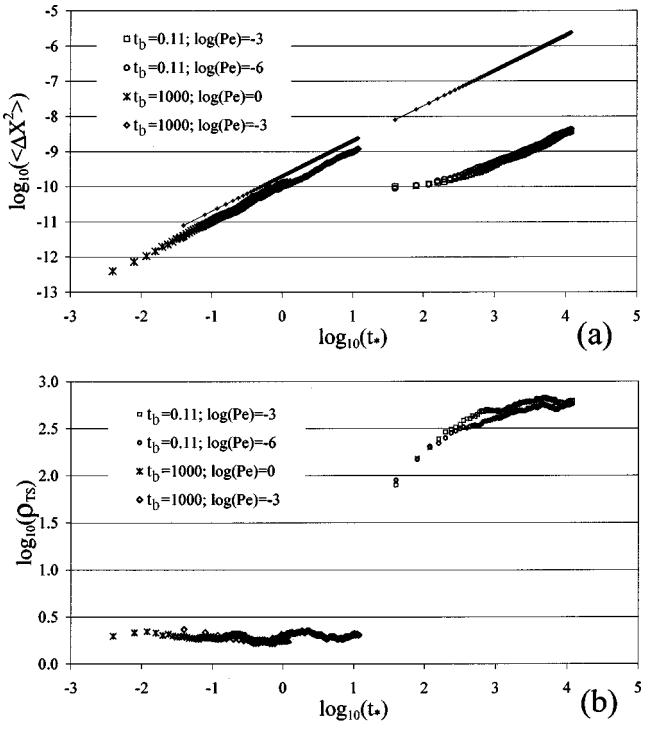

FIG. 13. Mean-square displacement $\langle \Delta x^2 \rangle_{\mathrm{sim}} = D^*_{\mathrm{eff}} t^{\gamma}_*$ variation with Péclet number $\mathrm{Pe} = v d / D_0$. Fixed $\alpha = 0.4$. t_b varies as indicated. (a) $\langle \Delta x^2 \rangle_{\mathrm{sim}} = D^*_{\mathrm{eff}} t^{\gamma}_*$, (b) benchmarking ratio against Taylor dispersion $\rho_{\mathrm{TS}} = \langle \Delta X^2 \rangle_{\mathrm{Taylor}} / \langle \Delta X^2 \rangle_{\mathrm{sim}}$. $\langle \Delta X^2 \rangle$ in (m^2).

be a retarded flow that progresses from subdispersive to Taylor dispersive for large t_*. This transition depends on both α and the value of t_b, being fast for large t_b and slow for small t_b.

V. DISCUSSION

The work presented herein is motivated by the desire to predict the evolution of genetic information in microbial populations within natural porous media. This work represents an important step towards this goal. Our earliest experiments on the propagation of antibiotic resistance and green fluorescent protein transfer (Wu [1]) have been conducted in auger plates and microflow cells. In the microflow cell, the transfer of genetic information takes place while the cells are adsorbed on the flow cell wall. The length of time the cell is adsorbed plays a direct role in the gene transfer process. We are thus motivated to study the hydrodynamics of microbes in microflow cells and their ''stickiness'' with respect to the walls. Brownian dynamic simulations of self motility in a convective field has been previously shown to adequately describe the behavior of microbes. We have added a twist to these simulations by considering sticky boundaries, where upon hitting a boundary the microbe sticks for a random length of time. This random length was governed by an α-stable distribution. The use of this distribution was motivated by four points: (i) α stables are renormalizable, (ii) α stables can have finite or infinite moments, (iii) α stables have heavy tails that highlight extreme events, and (iv) α stables are consistent with experiments.

The sensitivity has been studied in detail and the model can account for a great many sorptive processes with just a few parameters that may be estimated from direct measurements in the spirit of Drazer *et al.* [41]. The numerical experiments use Brownian dynamics in a convective flow between parallel plates with α-stable sorption waiting times. The parameters found to control transport limited sorption are α and, as in classical dispersion, $t_b = b^2/D_0$ which is the ratio of the square of the half width of the channel b to the diffusion coefficient of the bacteria D_0 that represents bacteria self motility. The α-stable waiting times distribution generates anomalous dispersion. The time evolution is different from that of a random walk with random stopping times as treated by Compte *et al.* [48] since stopping times here occur only upon collision with a wall instead of every diffusive step. As in classical Taylor dispersion with nonsorbing species, there exist a distinct behavior for short and long times. In classical dispersion, the threshold between the two regimes occurs at $t_* = t/t_b \approx 1$. In the case of α-stable sorptive species, this transition threshold depends on both α and t_b. When defining short and long times as limits for the process, it is useful to look at the number of wall collisions N_c which depends linearly on the average time spent in the aqueous phase t_a. Here, we have studied and reported in detail the dependence of t_a on t_b and α.

Universal scalings (with respect to dimensionless time $t_* = t/t_b$) for the mean position $\langle X \rangle = V^*_{\mathrm{eff}} t^{\theta}_*$ and mean-square displacement $\langle \Delta x^2 \rangle = D^*_{\mathrm{eff}} t^{\gamma}_*$ exist for long-time dispersion and the coefficients were obtained. Their values are consis-

tent and robust. The values of waiting time parameter α and the characteristic cross-channel motility time, t_b determine the nature of dispersion. If $\alpha<0.5$, there exist a combination of apparent subdispersive ($\gamma<1$) and apparent superdispersive ($\gamma>1$) dispersion regimes whose transition depends on the value of t_b. For $\alpha>0.5$, dispersion appears superdispersive and γ increases with t_b. Short- and long-time dispersion regimes may be consistently described with the same coefficients γ and D^*_{eff} for a wide range of conditions. Reversible and irreversible sorption can be modeled simultaneously with an appropriate choice for α. Values $\alpha<1$ allow deposition which occurs slower as α approaches one from below. These results are important for interpreting experiments and calibrating reactors where sorptive conditions widely vary in space.

ACKNOWLEDGMENTS

This work has been supported through a Showalter grant from the Purdue Research Foundation and NSF Grant No. 0003878-EAR. The authors thank Howard Berg for an insightful discussion on bacterial mechanics and for hosting J.H.C. during his sabbatical at Harvard.

APPENDIX A: α-STABLE DEVIATE GENERATOR

Stable deviates were generated with the Chambers-Mallows-Stuck algorithm. Since historically there have been inaccuracies in the literature surrounding this algorithm, we summarize it after developments by [49]. We do not include details about the construction of this particular fast generator of stable random variables as they can be found in [49] and [45] and citations therein.

A random variable Y is α stable if and only if its characteristic function is given by

$$\log_{10}\phi(s) = \begin{cases} -\sigma^\alpha|s|^\alpha\left\{1-i\beta\,\text{sgn(s)}\tan\dfrac{\pi\alpha}{2}\right\}+i\mu s & \text{if } \alpha\neq 1 \\ -\sigma|s|\left\{1+i\beta\,\text{sgn(s)}\dfrac{2}{\pi}\log_{10}|s|\right\}+i\mu s & \text{if } \alpha=1, \end{cases} \tag{A1}$$

where $\alpha\in(0,2]$ is the characteristic exponent, $\beta\in[-1,1]$ is the skewness, $\sigma>0$ is a scale parameter, and $\mu\in\mathbb{R}$ is a location parameter. We write $Y\sim S_\alpha(\sigma,\beta,\mu)$. When $\sigma=1$ and $\mu=0$ the distribution is called standard stable. Computer generation of a stable random variable follows

$$Y=\begin{cases} \sigma X+\mu & \text{if } \alpha\neq 1 \\ \sigma X+\dfrac{2}{\pi}\beta\sigma\log_{10}\sigma+\mu & \text{if } \alpha=1, \end{cases} \tag{A2}$$

where X is a standard stable random variable, that is, $X\sim S_\alpha(1,\beta,0)$. Now, to generate a standard stable deviate, follow the steps:

(1) Generate a random variable V uniformly distributed on $(-\pi/2,\pi/2)$ and an independent exponential random variable W

(2) For $\alpha\neq 1$, compute

$$X=S_{\alpha,\beta}\frac{\sin[\alpha(V+B_{\alpha,\beta})]}{[\cos(V)]^{1/\alpha}}\left(\frac{\cos[V-\alpha(V+B_{\alpha,\beta})]}{W}\right)^{(1-\alpha)/\alpha}, \tag{A3}$$

where

$$B_{\alpha,\beta}=\frac{\arctan\left[\beta\tan\left(\dfrac{\pi\alpha}{2}\right)\right]}{\alpha}, \tag{A4}$$

$$S_{\alpha,\beta}=\left[1+\beta^2\tan^2\frac{\pi\alpha}{2}\right]^{1/(2\alpha)}. \tag{A5}$$

(3) For $\alpha=1$, compute

$$X=\frac{2}{\pi}\left[\left(\frac{\pi}{2}+\beta V\right)\tan V-\beta\log_{10}\left(\frac{W\cos V}{\pi/2+\beta V}\right)\right]. \tag{A6}$$

The exponential deviates are computed by the inverse transform method based on uniform deviates. The uniform deviates needed were generated with an algorithm by [50].

APPENDIX B: LIMITING BEHAVIOR OF RANDOM WALKS

We collect here some analytic results which are useful in determining how to parametrize ρ, as well as some of the limiting behavior of random walks.

We first show that for a time discretized process that to have a positive amount of time on the boundary that

$$\frac{\epsilon}{(1-\epsilon)^2}=\frac{\rho}{\sqrt{\Delta t}}, \tag{B1}$$

where ϵ is the probability of staying on the boundary. From the central limit theorem or the basic properties of Brownian motion the time scale versus displacement scale is $B_{\text{st}}=\sqrt{s}B_t$. This means that if one discretizes the random walk in time and space and time steps are divided as Δt then the corresponding space discretization should be on the order of $\sqrt{\Delta t}$, so for example, if dividing time into intervals of length 0.01, one should divide space into intervals of length 0.1. Now if a random walk on the points $\{0,\sqrt{\Delta t},2\sqrt{\Delta t}\ldots$ is at zero at time zero and stays at zero with probability ϵ and if not at zero goes up or down $\sqrt{\Delta t}$ amount with probability 0.5, then one can ask how much time is the random walk at zero on the time interval $\{0,\Delta t,2\Delta t,\ldots,n/\Delta t\Delta t\}$ that is on $[0,n]$ where n is some large time.

The first question of interest is what is the distribution of the time that it takes for a bacteria executing a Brownian motion to first attach to a flow tube's boundary. If we assume that the flow is slow relative to the length of the flow tube then the answer is given by integrating the transition density.

That is, if we let $P(\tau>t)$ denote the probability that a microbe entering a flow cell has not hit the wall by time t, then with D as the cross-sectional area of the flow cell one has

$$P(\tau>t)=\int_D p(t,0,y)dy=\int_D \sum_{n=1}^{\infty} e^{-\lambda_n t}\phi_n(0)\phi_n(y)dy$$
$$=\sum_{n=1}^{\infty} e^{-\lambda_n t}\phi_n(0)\int_D \phi_n(y)dy=\sum_{n=1}^{\infty} c_n e^{-\lambda_n t},$$

where ϕ_n are Bessel functions, λ_n are zeroes of Bessel functions, and c_n are the integrals of the Bessel functions, all of which have been well tabulated. Notice that the long-time asymptotics are determined by the leading-order term in t.

If we do not assume that the velocity is slow relative to the length of the flow cell then there is a chance that a microbe might never hit the boundary before exiting. The probability of this event happening is approximately given (again letting D be the cross section)

$$P(\tau>t)=P(\tau_D>t \text{ or } \tau_{\text{end}}<t)\approx P(\tau_D>t)+P(\tau_{\text{end}}<t). \tag{B2}$$

The first of these is calculated as before and the latter can be approximated by a volume-averaged one-dimensional stochastic process.

Another question of interest is the expected amount of time a microbe spends on the wall. This is given by

$$\langle \tau_{\text{wall}}\rangle=\langle \rho K_t\rangle \text{ the local time of the process}$$
$$=\rho\langle K_t\rangle\approx\rho\frac{|\partial\Omega|}{|\Omega|}\langle T\rangle$$
$$=\rho\langle K_t\rangle\approx\rho\frac{|\partial\Omega|}{|\Omega|}\frac{\text{length}}{\langle v\rangle}. \tag{B3}$$

Here, T is the time inside the flow cell.

The final question we are interested in is what is the distribution of the time on the wall for a microbe in a flow chamber given that it starts on a wall. This is an important question, since if one is interested in introducing genetic information into a microbial community the transfer of genes takes place when microbes come into contact, a process most likely to occur on boundaries. With $\tilde{\tau}$ representing the amount of time on the boundary we want

$$P(\tilde{\tau}>t|\tilde{\tau}>0)\approx P\left(K_T>\frac{t}{\rho}\right)\approx P\left(K_{(\text{length})/\langle v\rangle}>\frac{t}{\rho}\right). \tag{B4}$$

This last quantity is finally calculated [using Eq. (20)] as the square root of an exponential distribution.

APPENDIX C: EXTREME EVENTS TREATMENT

To study reversible or irreversible sorption, we differentiate between adhesion events as follows. We decide which events j are extreme for particle i by defining a cutoff value for attachment time t_f, such that the duration t_s^{ij} is considered an extreme value if $t_s^{ij}>t_f$. Table II shows a set of cutoff values for different values of α selected for the following analysis. The third line in Table II is the total mass (probability) under the sorption time probability density function up to the cutoff time t_f [51]. The value $P(\|T\|\leqslant t_f)$ is the probability of occurrence of a nonextreme sorption time event j for particle i of duration t_{s1}^{ij}, and $1-P(\|T\|\leqslant t_f)$ is the probability of occurrence of an extreme sorption time event upon collision (duration t_{s2}^{ij}). Average times t_{s1} and t_{s2} are computed as

$$t_{s1}=\frac{1}{N_p}\sum_{i=1}^{N_p}\sum_{j=0}^{N_c} t_s^{ij}\Pi(t_s^{ij}), \tag{C1a}$$

$$t_{s2}=\frac{1}{N_p}\sum_{i=1}^{N_p}\sum_{j=0}^{N_c} t_s^{ij}[1-\Pi(t_s^{ij})], \tag{C1b}$$

where i and j are counting variables for particles and collisions, respectively, N_p is the number of particles, N_c is the average number of collisions against the wall, and $\Pi(t_s^{ij})$ is an indicator function for the occurrence of an extreme event

$$\Pi(t_s^{ij})=\begin{cases}1 & \text{if } t_s^{ij}<t_f\\ 0 & \text{otherwise.}\end{cases} \tag{C2}$$

[1] Y. Wu, MS thesis, Purdue University, 2002 (unpublished).
[2] H. Berg, Phys. Today **53**, 24 (2000).
[3] M. Fletcher, in *Bacterial Adhesion Molecular and Ecological Diversity: Molecular and Ecological Diversity*, edited by M. Fletcher (Wiley, New York, 1996), pp. 1–24.
[4] M. Dawson, B. Humphrey, and K. Marshall, Curr. Microbiol. **6**, 195 (1981).
[5] M. van Loosdrecht, J. Lyklema, W. Norde, G. Schraa, and A. Zehnder, Appl. Environ. Microbiol. **53**, 1898 (1987).
[6] M. van Loosdrecht, J. Lyklema, W. Norde, and A. Zehnder, Microbiol. Rev. **54**, 75 (1990).
[7] M. Fletcher and K. Marshall, in *Advances in Microbial Ecology*, edited by K. Marshall (Plenum, New York, 1982), pp. 199–236.
[8] C. Chen, M. Reinsel, and R. Mueller, Biotechnol. Bioeng. **44**, 263 (1994).
[9] M. Widdowson, Water Resour. Res. **27**, 1375 (1991).
[10] P. Jaffe and S. Taylor, Water Resour. Res. **28**, 1483 (1992).
[11] Z. Adamczyk, P. Warszyński, L. Szyk-Warszyńska, and P. Weroński, Colloids Surf., A **165**, 157 (2000).
[12] H. Berg and L. Turner, Biophys. J. **58**, 919 (1990).
[13] G. Viswanathan, V. Afanasyev, S. Buldyrev, S. Havlin, M. da Luz, E. Raposo, and H. Stanley, Physica A **282**, 1 (2000).

[14] R. Bearon and T. Pedley, Bull. Math. Biol. **62**, 775 (2000).
[15] M. Bees and N. Hill, Phys. Fluids **10**, 1864 (1998).
[16] S. Kuo and J. McGrath, Nature (London) **407**, 1026 (2000).
[17] A. Samuel, J. Petersen, and T. Reese, BMC Microb. **1**, 4 (2001).
[18] S. Biondi, J. Quinn, and H. Goldfine, AIChE J. **44**, 1923 (1998).
[19] B. Phillips, J. Quinn, and H. Goldfine, AIChE J. **40**, 334 (1994).
[20] H. Berg and D. Brown, Nature (London) **239**, 500 (1972).
[21] H. Othmer, S. Dunbar, and W. Alt, J. Math. Biol. **26**, 263 (1988).
[22] M. Rivero, R. Tranquillo, H. Buettner, and D. Lauffenberger, Chem. Eng. Sci. **44**, 2881 (1989).
[23] T. Camesano and B. Logan, Environ. Sci. Technol. **32**, 1699 (1998).
[24] H. Rijnaarts, W. Norde, E. Bouwer, J. Lyklema, and A. Zehnder, Environ. Sci. Technol. **30**, 2877 (1996).
[25] S. Whitaker, Chem. Eng. Sci. **47**, 1677 (1992).
[26] J. Meinders, H. van der Mei, and H. Busscher, J. Colloid Interface Sci. **176**, 329 (1995).
[27] N. Yee, J. Fein, and C. Daughney, Geochim. Cosmochim. Acta **64**, 609 (2000).
[28] D. McCaulou, R. Bales, and R. Arnold, Water Resour. Res. **31**, 271 (1995).
[29] E. Murphy and T. Ginn, Hydrogeol. J. **8**, 142 (2000).
[30] M. Hermansson, Colloids Surf. B: Biointerfaces **14**, 105 (1999)
[31] H. Busscher, A. Poortinga, and R. Bos, Curr. Microbiol. **37**, 319 (1998).
[32] D. Ermak and J. McCammon, J. Chem. Phys. **69**, 1352 (1978).
[33] J. Bafaluy, B. Senger, J. Voegel, and P. Schaaf, Phys. Rev. Lett. **70**, 623 (1993).
[34] A. Boyd and A. Chakrabarty, Appl. Environ. Microbiol. **60**, 2355 (1994).
[35] C. Graham, Ann. Inst. H. Poincaré Probab. Statist. **24**, 45 (1988).
[36] A. Borodin and P. Salminen, *Handbook of Brownian Motion: Facts and Formulae* (Birkhäuser Verlag, Basel, 1996).
[37] D. Lepingle, Math. Comput. Simul. **38**, 119 (1995).
[38] S. McEldowney and M. Fletcher, Arch. Microbiol. **148**, 57 (1987).
[39] O. Pictet, M. Dacorogna, and U. Müller, in *A Practical Guide to Heavy Tails*, edited by R. Adler, R. Feldman, and M. Taqqu (Birkhäuser, Boston, 1998), pp. 283–310.
[40] *A Practical Guide to Heavy Tails* (Ref. [39]).
[41] G. Drazer, M. Rosen, and D. Zanette, Physica A **283**, 181 (2000).
[42] G. Drazer and D. H. Zanette, Phys. Rev. E **60**, 5858 (1999).
[43] M. O. Vlad, G. Cerofolini, and J. Ross, Phys. Rev. E **62**, 837 (2000).
[44] S. E. Silliman, R. Dunlap, M. Fletcher, and M. A. Schneegurt, Water Resour. Res. **37**, 2699 (2001).
[45] J. P. Nolan, Math. Comput. Modell. **29**, 229 (1999).
[46] H. Brenner and D. A. Edwards. *macrotransport Processes* (Butterworth-Heinemann, London, 1983).
[47] O. Bychuk and B. Oshaughessy, Phys. Rev. Lett. **75**, 1795 (1995).
[48] A. Compte, R. Metzler, and J. Camacho, Phys. Rev. E **56**, 1445 (1997).
[49] R. Weron, Stat. Probabil. Lett. **28**, 165 (1996).
[50] M. Matsumoto and T. Nishimura, ACM Trans. Model. Comput. Simul. **8**, 3 (1998).
[51] G. Samorodnitsky and M. Taqqu, *Stable Non-Gaussian Random Processes: Stochastic Models with Infinite Variance* (Chapman & Hall, New York, 1994).